Available online at www.sciencedirect.com
ScienceDirect
Trans. Nonferrous Met. Soc. China 32(2022) 3388−3403
Transactions of Nonferrous Metals Society of China
www.tnmsc.cn

Effects of microwave radiation on dynamic compressive properties of basalt

Tu-bing YIN, Fei-yan JIN, Qiang LI, Xi-bing LI

School of Resources and Safety Engineering, Central South University, Changsha 410083, China

Received 15 July 2021; accepted 29 December 2021

Abstract: The dynamic mechanical properties of basalt affected by microwave were investigated by performing dynamic compressive tests using the SHPB system. Meanwhile, the thermal damage of the treated basalt was characterized by ultrasonic non-destructive testing and nuclear magnetic resonance technology. The results show that with the increase of microwave power and exposure time, the P-wave velocity, dynamic compressive strength and elastic modulus decrease continuously, and the dynamic failure mode tends to be a more complex fracturing. The increase in microwave power and exposure time can enhance the temperature difference and transfer coefficient among minerals, hence intensifying the rock damage induced by thermal shock.

Key words: microwave radiation; nuclear magnetic resonance (NMR); dynamic compressive properties; thermal damage

1 Introduction

The mechanical excavating technology has been widely used in mining and tunneling industries due to the advantages of efficiency, accuracy and safety [1,2]. But there are great challenges such as high costs and high technical requirements when excavating extremely hard and abrasive rocks using traditional mechanical rock-breaking methods [3,4]. In recent years, some innovative rock-breaking techniques, such as water jet, laser, plasma, electron beam and microwave, have shown great potential applications [1,5,6]. Among them, the microwave-assisted rock breaking technique has been widely regarded as a prospective preconditioning method with environmental friendliness and low energy consumption.

Minerals in rocks have different thermal expansion and microwave absorption capabilities. Generally, rocks with better microwave absorption minerals can be heated up quickly [7,8]. CHEN et al [9] and LU et al [8] investigated the general behaviors of rock-forming minerals exposed to microwave radiation. The research illustrated that minerals like magnetite, enstatite and chalcopyrite can be classified as strong microwave absorbers, whereas feldspar, quartz and marble are considered to be weak microwave absorbers. The sensitivity of minerals to microwave is determined by their permittivity. ALI and BRADSHAW [10] found that the mineralogical composition and texture of the rock affected the thermodynamic response to microwave radiation.

To investigate the physico-mechanical properties and microstructure of rocks after microwave radiation, scholars have conducted a series of studies theoretically, experimentally and numerically. HASSANI et al [11] illustrated that microwave radiation reduced the uniaxial compressive strength and Brazilian tensile strength of basalt by 40% (exposure to 5 kW for 65 s) and

Corresponding author: Qiang LI, Tel: +86-18361228501, E-mail: qli2018@126.com
DOI: 10.1016/S1003-6326(22)66027-8

by 20%−30% (exposure to 1.2 kW for 120 s), respectively. KINGMAN et al [12] concluded that the higher the microwave power and the longer the exposure time, the higher the magnitude of the strength reduction of the rock. LI et al [13] investigated the degeneration of fracture toughness of granite subjected to microwave heating, meanwhile, their acoustic emission (AE) and digital image correlation (DIC) verified the enhancement of treated granite. Both experimental [7,11,14] and numerical simulation results [15,16] lead to the same conclusion: under the same input energy, higher power density and shorter exposure time have a greater effect on the rock strength degradation. Recently, X-ray diffraction (XRD), X-ray photoelectron spectroscopy (XPS) [17], computed tomography (CT) [18] and scanning electron microscopy (SEM) techniques [11,19] were utilized to observe the microstructure of the rock after microwave radiation. OMRAN et al [17] found that after microwave radiation, the crystallinity of hematite increased significantly by XRD and XPS. Some researchers [15,16,20,21] found that the original cracks and voids developed for a short exposure time at low power density. With the increase of the exposure time and microwave power, new intergranular and transgranular microcracks generated successively in the rock. In addition, WANG et al [15] revealed that the tensile stress is the main cause of initial breakage, and the thermal stress mainly occurred around the boundary of the microwave-sensitive minerals by finite element simulation.

Four types of mechanical rock breaking methods are widely used in mining and tunneling: cutting rock breaking under static load, dynamic rock breaking under impact load, combined rock breaking under impact and cutting load, and combined rock breaking under dynamic and static compression load [22,23]. LI et al [24] found that the rock cuttability decreased under the biaxial confining stress compared with the stress-free conditions. This can lead to a higher requirement for thrust force to cut deep rock. ERGIN and ACAROGLU [25] and YANG et al [26] indicated that dynamic loading can improve rock cuttability, insertion depth, and breaking efficiency. Compared with the stand-alone static or cutting rock breaking techniques, the dynamic rock breaking technique has the advantages of high drilling efficiency, high energy utilization, and low drilling cost. Therefore, it is of great significance to investigate the effects of microwave radiation on the dynamic mechanical properties of hard rocks.

Aiming to study the damage mechanism and dynamic mechanical properties of basalt under microwave radiation, ultrasonic detecting tests, nuclear magnetic resonance (NMR) tests and impact tests were conducted on basalt samples before and after the microwave radiation. The microscopic damage of basalt was determined and characterized by ultrasonic detecting technique and NMR technique. A series of impact tests were carried out by a modified Split Hopkinson Pressure Bar (SHPB) to determine the dynamic compressive strength and dynamic deformation characteristics. Meanwhile, the dynamic failure patterns and fracture mechanisms of microwave-treated basalt were analyzed and compared to reveal the influence of microwave on the dynamic rock fragmentation. Finally, we revealed the microscopic damage mechanism of basalt under microwave radiation.

2 Rock material and specimen preparation

2.1 Material description

The rock material collected for this study is a fine-grained basalt from Inner Mongolia, China. The mineralogical composition of the basalt was determined by X-ray diffraction (XRD), and the XRD pattern shows that the basalt used in this study is mainly composed of four minerals, feldspar (73.72%), pyroxene (18.67%), montmorillonite (6.25%) and quartz (1.36%), as shown in Fig. 1. Their microwave absorption behaviors were

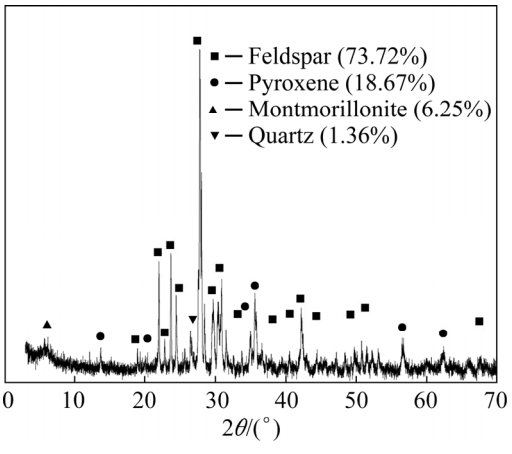

Fig. 1 XRD pattern of basalt

determined based on the previous investigation by LU et al [8], as presented in Table 1. Moreover, Fig. 2 shows the optical microscopy images of this basalt under a Zeiss polarized light microscope. It can be observed that the basalt is gray-black with a fine intergranular structure. Feldspar is a more euhedral-granular, plate columnar structure, and most of its particle size is less than 0.3 mm × 0.1 mm. Pyroxene is euhedral and hypidiomorphic granular, with a granular structure, and most of its mineral particles are below 0.5 mm. In addition, it can be found that some irregular pores are distributed in the rock matrix. The physical and mechanical properties of basalt are presented in Table 2.

Table 1 Mineralogical compositions by XRD test

Mineral	Basalt content/ vol.%	Microwave absorbing property	Grain size/mm
Quartz	1.36	Very weak	0.06−0.4
Feldspar	73.72	Weak	0.05−0.4
Montmorillonite	6.25	Weak	0.1−0.4
Pyroxene	18.67	Strong	0.1−0.8

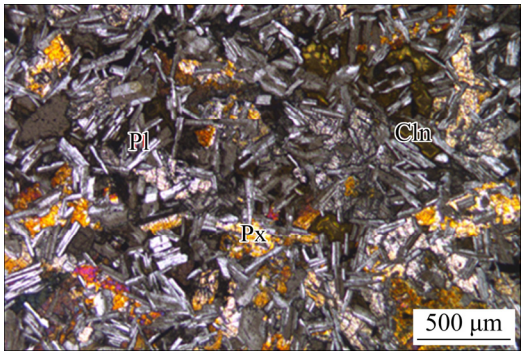

Fig. 2 Petrographic microscopy image of basalt (Pl−Feldspar; Px−Pyroxene; Cln−Montmorillonite)

2.2 Specimen preparation

In this study, all samples were prepared in accordance with the standard method recommended by the International Society for Rock Mechanics and Rock Engineering (ISRM) [27]. To ensure high geometric integrity and lithofacies uniformity, all samples were drilled and cut from the same fresh rock block. The basalt samples were made into cylinders with a diameter of 50 mm and a height of 50 mm for dynamic mechanical testing. After that, the surfaces were polished to ensure that the two end planes of the sample were parallel with an accuracy of ±0.05 mm and the surface roughness was less than 0.02 mm. In addition, the P-wave velocities were measured and the specimens with large deviations in P-wave velocity were discarded.

3 Experimental

3.1 Experimental procedure

After sample preparation, the basalt samples were divided into three groups corresponding to three microwave power levels of 2, 4, and 6 kW, respectively. The irradiation time interval for each power level was 30 s, and the microwave radiation was ended when the samples showed visible cracks. Firstly, the rock porosity and pore distribution were measured by an NMR apparatus, and then the sample was dried in a drying oven to avoid the disturbance of moisture during the microwave radiation. It is worth noting that a single drying and saturation treatment has almost no effect on the properties of the rock [28]. After that, the sample was treated in an industrial microwave oven. Once being irradiated to the predetermined time, the surface temperature of all samples will be accurately measured using an AS872 infrared thermometer, and the temperature in the interior will be also measured for burst samples. After the sample was slowly cooled down to ambient temperature in the microwave oven, the P-wave velocity, porosity and pore distribution of basalt samples were measured again. Finally, the dynamic compressive tests were conducted by a modified SHPB system.

3.2 Microwave testing system

Microwave is a type of electromagnetic wave with frequencies ranging from 0.3 to 300 GHz.

Table 2 Physical and mechanical properties of basalt

Elastic modulus, E/GPa	Poisson's ratio, μ	P-wave velocity, V/(m·s^{-1})	Density, ρ/(g·cm^{-3})	Compressive strength, σ_c/MPa
43.64	0.25	5135.19	2.67	186.48

Specifically, the frequency of microwave in this study was 2.45 GHz. The industrial microwave oven with a multi-mode cavity was provided by the Megmeet Co., in Zhuzhou, China, which consists of a microwave generator, a monitoring system and a control system. The microwave generator consists of six independently operating magnetrons with a power of 1kW, and the output power of this microwave oven can reach up to 6 kW.

When the material is subjected to microwave radiation, a dynamic electric field is generated and then the dipoles begin to rotate and move with the electric field, as shown in Fig. 3. The high-frequency reciprocating motion of the dipole molecules generates internal frictional heat and then increases the temperature of the basalt. The sensitivity of a material to microwave depends greatly on its complex permittivity (ε). The dielectric properties can be described by

$$\varepsilon = \varepsilon_0 \left(k' + \mathrm{i}k''\right) \tag{1}$$

where k' and k'' are the real part and imaginary part of the relative dielectric constant, respectively, and ε_0 is the permittivity of free space. The microwave absorption capacity of the rock in an electro-magnetic field can be calculated by the following equation [6,11,12]:

$$P = 2\pi f \varepsilon_0 \varepsilon'' E'^2 \tag{2}$$

where P is the loss power density deposited in the sample, f is the microwave frequency, ε'' is the loss factor of the material, and E' is the electric field strength.

3.3 Measurement of rock porosity by NMR technology

Nuclear magnetic resonance (NMR) technology has been widely used to detect pore structures due to its non-destructive, efficient and accurate advantages. The principle of the NMR test is tracing the hydrogen nuclei of water inside the pores. Generally, surface relaxation, free relaxation and molecular self-relaxation exist simultaneously, but the latter two can be ignored in this test. The relationship between the crosswise transverse relaxation time T_2 and the pore-throat radius can be expressed by the following formula [29]:

$$\frac{1}{T_2} = \rho_2 F_s \frac{1}{r} \tag{3}$$

$$r = CT_2 \tag{4}$$

where ρ_2 is the transverse surface relaxivity; F_s is the geometrical shape factor; r is the pore radius; C is a constant. The porosity and T_2 spectrum can be obtained and analyzed by Core analysis software.

3.4 Measurement of rock dynamic strength by SHPB system

The modified split Hopkinson Pressure Bar (SHPB) was widely used to study the dynamic mechanical properties of materials at high strain rates of 10^1 to 10^4 s^{-1}. As shown in Fig. 4, the test system consists of a gas gun, a cone-shaped striker, an incident bar, a transmitted bar, an absorption bar and a momentum trap. The developed cone-shaped

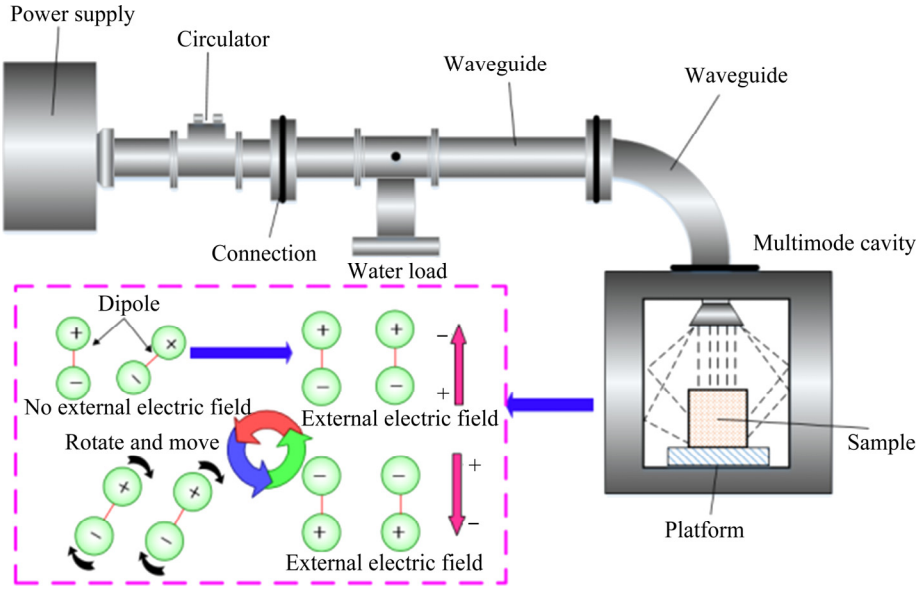

Fig. 3 Microwave heating system and typical phases of microwave heating test

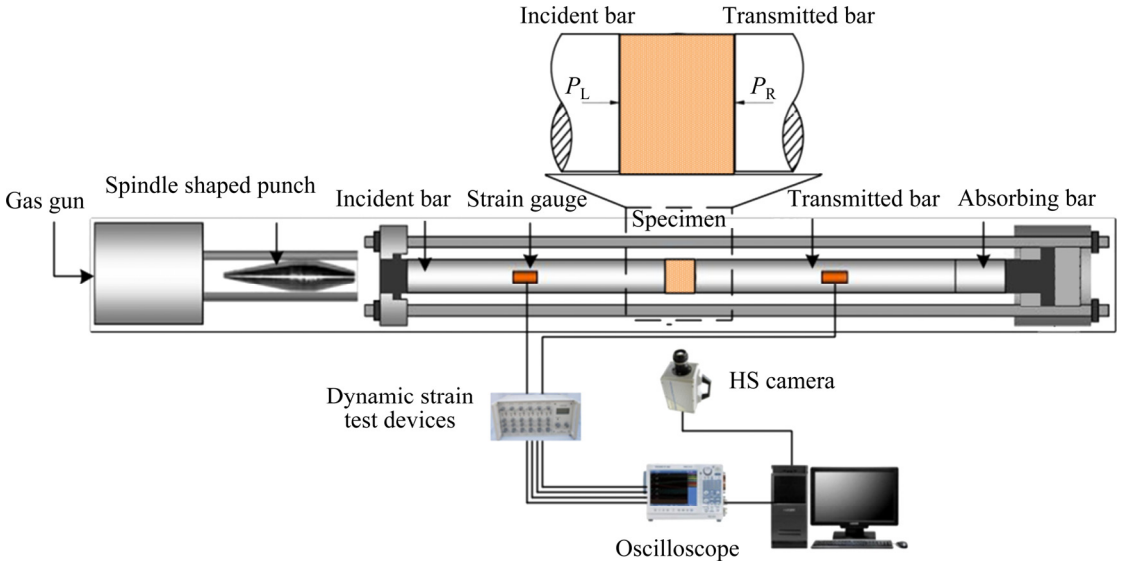

Fig. 4 Apparatus of SHPB system for dynamic loading

striker can generate a half-sine wave to eliminate P−C oscillation [30]. The bars and the striker are made of high strength 40Cr alloy with a density of 7800 kg/m^3, an elastic modulus of 250 GPa and a yield strength of 800 MPa. Two pairs of strain gauges are glued on the incident and transmitted bars, respectively, collecting and converting the wave into strain signals to determine the force history. The mechanical properties of the specimens can be calculated through analysis of the voltage in the strain gauge. According to the one-dimensional elastic wave theory, the stress σ, strain ε and the strain rate $\dot{\varepsilon}$ of the specimen can be obtained by the following formulas [31,32]:

$$\sigma(t)=\frac{A_e}{2A_s}E_e\left(\varepsilon_I(t)+\varepsilon_R(t)+\varepsilon_T(t)\right) \tag{5}$$

$$\varepsilon(t)=\frac{C_e}{L_s}\int_0^t\left(\varepsilon_I(t)-\varepsilon_R(t)-\varepsilon_T(t)\right)\mathrm{d}t \tag{6}$$

$$\dot{\varepsilon}(t)=\frac{C_e}{L_s}\left(\varepsilon_I(t)-\varepsilon_R(t)-\varepsilon_T(t)\right) \tag{7}$$

where A_e, C_e and E_e are the cross-sectional area, wave velocity and elastic modulus of the bars, respectively; A_s and L_s are the cross-sectional area and length of the specimen respectively; $\varepsilon_I(t)$, $\varepsilon_R(t)$ and $\varepsilon_T(t)$ respectively represent the incident, reflection, and transmission strains of the bars at time t.

In this study, a high-speed camera operating at 80000 frames per second was used to observe the crack initiation and propagation of basalt specimens during dynamic tests.

4 Results

4.1 Temperature characteristics

The relationship between the surface temperature of the basalt specimens subjected to microwave radiation and exposure time is shown in Fig. 5. As can be seen, the surface temperature increases approximately linearly with the increasing exposure time, and the curve with a higher power level has a larger slope, which means a higher heating rate. Specifically, the average heating rate is 1.65 °C/s at 2 kW, 1.98 °C/s at 4 kW, and 3.58 °C/s at 6 kW, respectively.

Once the basalt samples burst, we simultaneously measured the temperatures on the surface and in the interior within a few seconds after the end of the microwave radiation. We found that the surface temperature of the burst sample was apparently lower than that of the interior, as shown in Table 3. This observation can be interpreted as heat dissipation and run-away effect [14]. The existence of heat exchange between surrounding air and the basalt leads to heat dissipation on the rock and then a decrease in surface temperature. Furthermore, the increase in k'' with temperature intensifies the permittivity of the internal minerals, thereby enhancing the molecular polarization. As a consequence, the inner region is hotter than the surface.

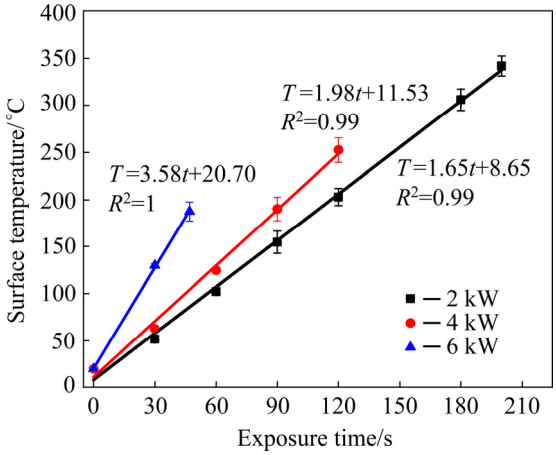

Fig. 5 Variations of surface temperature with microwave exposure time

Table 3 Heating conditions of basalt after microwave radiation

Power/kW	Heating rate/(°C·s^{-1})	Burst time/s	Burst temperature/°C		Input energy/kJ
			Surface temperature	Interior temperature	
2	1.65	200	342	405	400
4	1.98	120	253	340	360
6	3.58	47	188	245	235

The input energy equals input power multiply exposure time

4.2 Variation in P-wave velocity

The variations of normalized P-wave velocity (V_p/V_{p_0}) with exposure time of the basalt under microwave radiation are shown in Fig. 6. It can be seen that the P-wave velocity of basalt decreases gradually with increasing time at three power levels. Moreover, it clearly shows that the higher the microwave power, the more degeneration of the P-wave velocity. After microwave radiation, the internal structure and material properties of basalt underwent various changes, and a large number of microcracks appeared in the basalt, which caused complex reflection and scattering of the ultrasonic waves in the rock matrix. Meanwhile, the propagation velocity of ultrasonic wave in air is much lower than that in solids. Therefore, the P-wave velocity of basalt decreases.

Compared with the results of P-wave velocities of the other four rocks [14,33,34], as shown in Fig. 6, it is clearly illustrated that the overall trend of V_p is basically consistent with that of basalt. However, under the same heating conditions, every type of rock has its unique response to microwave, which is mainly related to the mineralogical compositions and structures of the rocks. For example, after being irradiated at 2 kW for 60 s, the reduction of V_p in gabbro was much higher than that of basalt. This is mainly because the average contents of strong microwave absorbers of gabbro and basalt are 31% (pyroxene 25%, K-feldspar 5%, biotite 1%) and 18.67% (pyroxene18.67%), respectively. In addition, it can be seen that the heating rates of sandstone and granite are similar, which can be attributed to the close value of k'' of minerals. Interestingly, the P-wave velocity of the sandstone shows a fluctuant trend, while the P-wave velocities of basalt and granite decrease continuously. This can be attributed to the combined effect of crack closure induced by mineral expansion and crack propagation induced by uneven deformation.

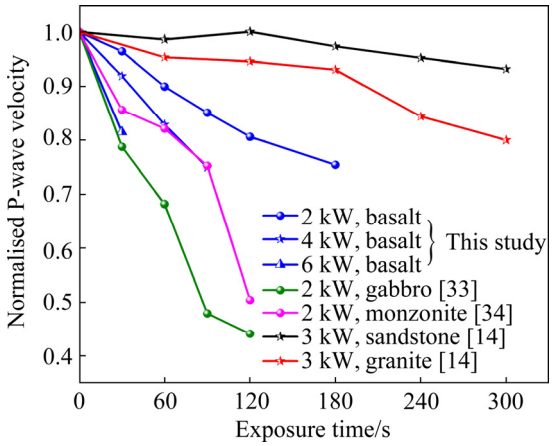

Fig. 6 Variations of normalized P-wave velocity of basalt heated with exposure time

We all know that the ultrasonic P-wave velocity can indirectly indicate the degree of weakening of the sample by microwave treatment. According to elastic strain theory, a damage factor (D) is defined to evaluate the overall damage degree of the samples after microwave radiation [35]:

$$D = 1 - \left(V_p / V_{p_0}\right)^2 \quad (8)$$

where V_{p_0} and V_p are the P-wave velocities of basalt samples before and after microwave radiation, respectively. The variations in thermal damage of basalt and other four types of rocks with exposure time are shown in Fig. 7. Overall, D increases linearly with exposure time, and D is larger for basalt samples after higher power-microwave

radiation for equal exposure time. In addition, it can be found that the variation of damage factor of all rocks can be fitted by a linear equation. This indicates that the generation and accumulation of microwave-induced thermal damage within the rock are relatively stable before the rock is completely destroyed.

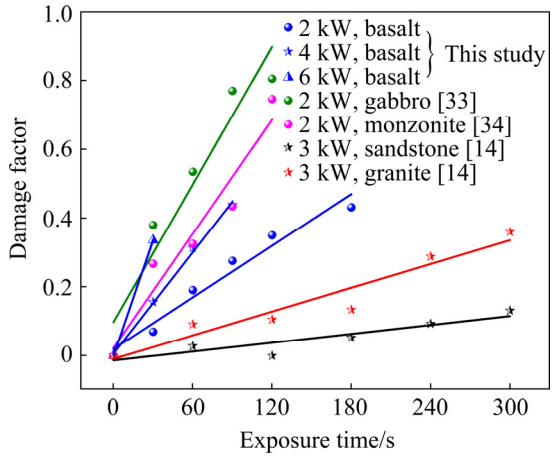

Fig. 7 Variations of thermal damage of basalt heated with exposure time

4.3 Dynamic compressive properties and failure patterns

4.3.1 Verification of dynamic stress equilibrium

For a successful dynamic compression test, the stresses at the incident (In) and transmitted (Tr) ends of the sample should be approximately equal before failure, that is, the sample is in a state of stress equilibrium during the deformation. According to the SHPB test principles, the end force of the sample can be obtained from the test signals on the elastic bars. Figure 8 shows the stress history of a typical dynamic compressive

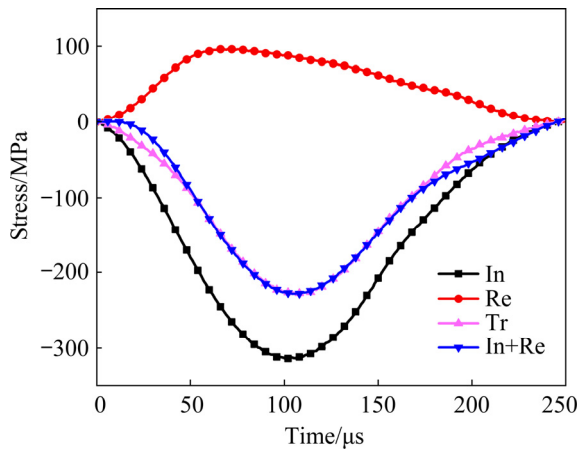

Fig. 8 Dynamic stress balance check for typical compression test (Re−Reflected)

experiment, in which the sample reaches the state of stress equilibrium. In this study, the dynamic stress equilibrium state of all samples was strictly verified.

4.3.2 Variation in dynamic properties

In all dynamic experiments, the impact pressure is maintained at 0.93 MPa, which corresponds to an incident velocity of 20 m/s. Figure 9 shows the dynamic stress−strain curves of basalt before and after microwave radiation. It can be found that, after microwave radiation, the

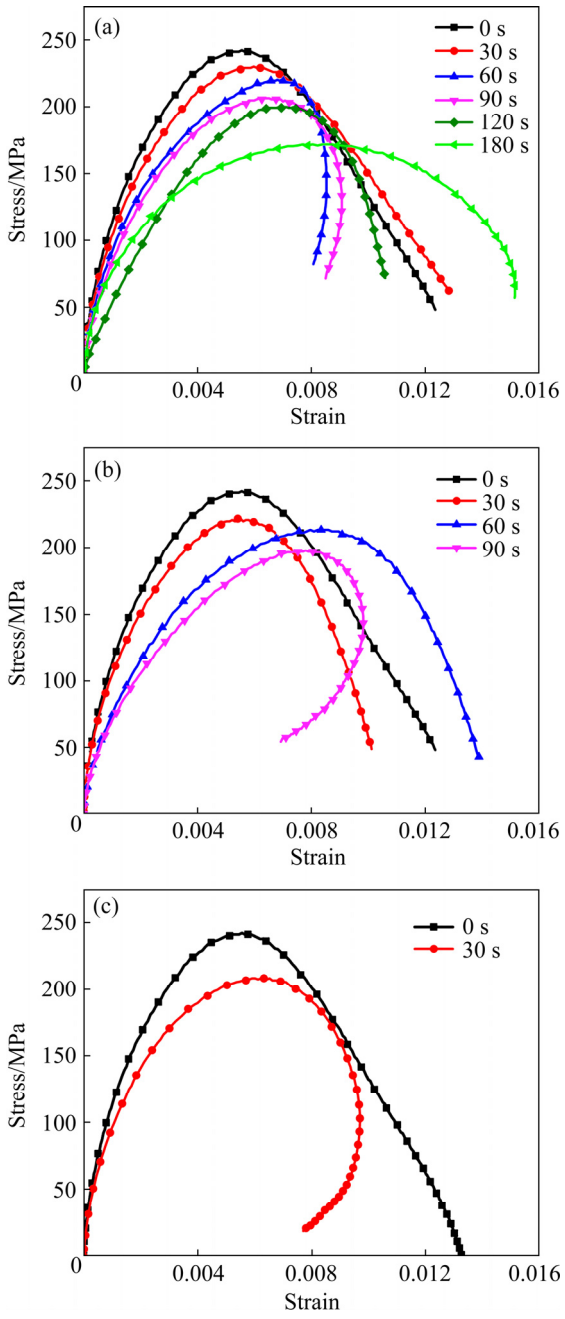

Fig. 9 Stress−strain curves of basalt under impact loading after microwave radiation: (a) 2 kW; (b) 4 kW; (c) 6 kW

dynamic stress−strain curves of all samples can be roughly divided into three stages: elastic, yield, and failure stage. Under compressive stress waves, the basalt directly entered the elastic stage without closing effect owing to the high strain rate. When the applied stress exceeded the yield strength, the tensile microcracks initiated at the tip of the original cracks along the loading direction, then gradually propagated, expanded and coalesced until the total failure of the sample [36]. Compared with untreated samples, the elastic deformation stages of microwave-treated basalt samples become shorter and the elastic modulus generally becomes smaller. Besides, both the yield strength and dynamic compressive strength of treated samples decrease to varying extents. After microwave radiation, the cementation between particles in basalt was degraded gradually, accordingly, the stability of the rock skeleton declined due to the mismatch deformation. This weakened the stiffness of the basalt samples and reduced the impact stress required to reach the yield stage.

Figure 10 further plots the variations of dynamic compressive strength of basalt subjected to different microwave power levels and exposure time. At all microwave power levels, the strength of samples decreases linearly with the increasing exposure time. Microwave radiation at a higher power level has more obvious advantages with regard to the reduction of strength. After being treated at 2 Kw for 180 s, the strength reduction was approximately 29.49%, while at 4 kW for 90 s and 6 kW for 30 s, the strength reduction was 19.70% and 14.40%, respectively.

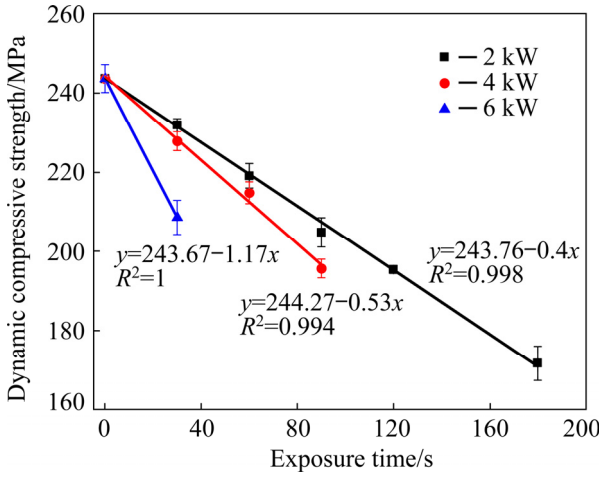

Fig. 10 Relationship between dynamic compressive strength and exposure time of microwave-treated basalt

Compared with basalt, the dynamic mechanical properties of sandstone after microwave treatment are less degraded. Specifically, After being treated at 2 and 4 kW for 90 s, the dynamic compressive strength of basalt decreased by 16% and 20%, respectively. While the dynamic compressive strength of sandstone was reduced by 8% and 17% after being treated at 3 kW and 5 kW for 90 s, respectively [37]. Although a higher power level is used, the dynamic compressive strength of sandstone after microwave treatment is significantly lower than that of basalt. This can be attributed to the fact that the content of strong absorbers in basalt (pyroxene 18.67%) is significantly greater than that of sandstone (calcite 5.53%, hematite 4.73%).

4.3.3 Failure patterns of basalt in dynamic compressive tests

In order to deeply understand the macroscopic failure mechanism, the fracturing behaviors of basalt during impact tests were captured by a high-speed camera, as shown in Fig. 11. In general, it can be seen that with the increase of exposure time, the severer damage and smaller debris of the basalt sample can be found, indicating that microwave pre-treatment significantly promotes the rock fragmentation. According to the failure processes of basalt in dynamic compressive tests, two typical final failure modes can be observed, as shown in Fig. 12.

Type I: Axial splitting. Under compact loading, basalt samples were split into a few fragments along the axial direction of the sample, which can be attributed to the tensile stress caused by the Poisson effect [36]. This failure pattern can be observed on untreated samples and samples treated by microwave at lower power levels for shorter exposure time. For untreated samples, the main crack was composed of one or more parallel cracks along the axial, which is a typical splitting failure mode. For basalt samples subjected to microwave radiation at lower power levels for shorter exposure time (at 2 kW for 30−60 s and at 4 kW for 30 s), the failure mode was similar to that of the untreated basalt. The difference was that the main crack presented a more tortuous path during the propagation process, indicating that the final failure of basalt was controlled by the initial microwave-induced microcracks.

Type II: Crack propagation in the axial and perpendicular to the axial direction. After the

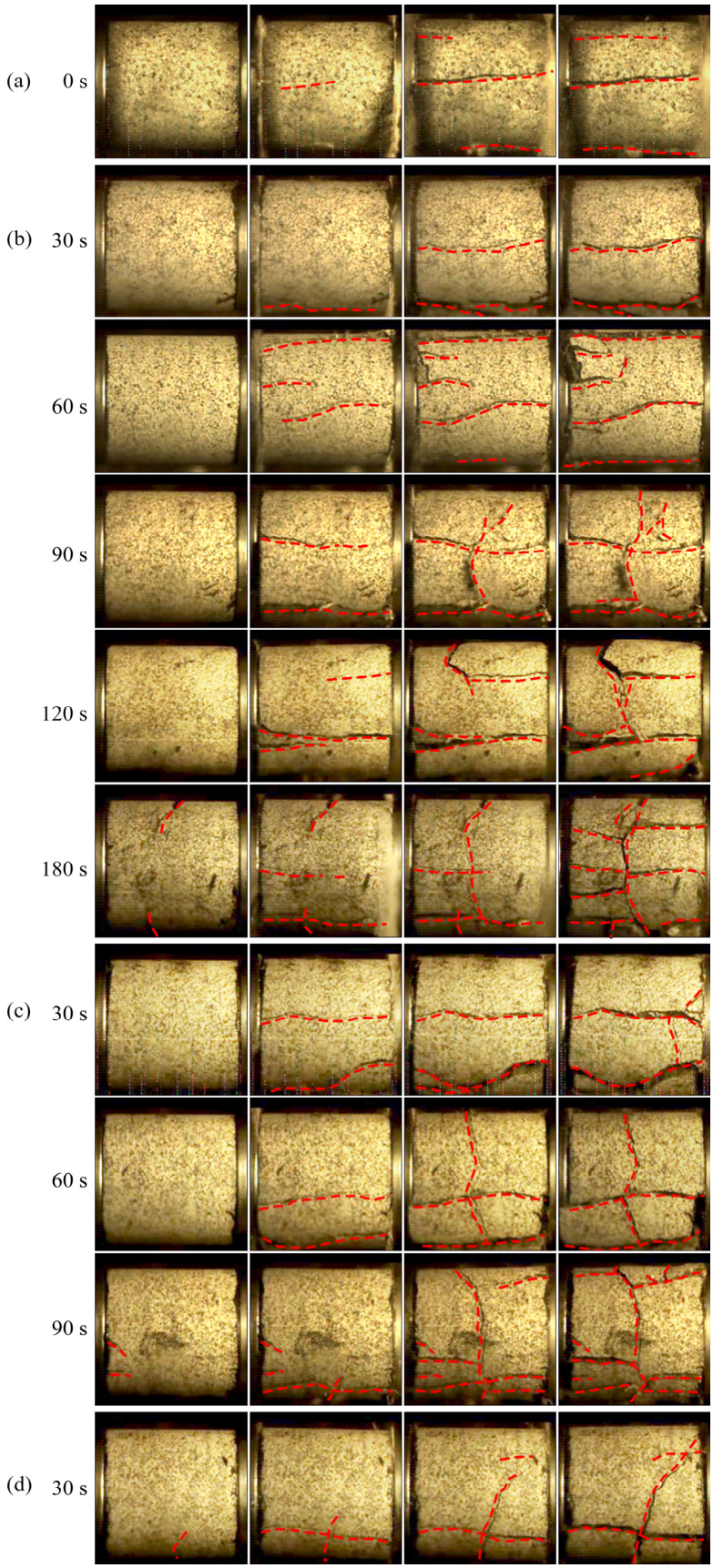

Fig. 11 Failure processes of basalt in dynamic compressive tests captured by high-speed camera: (a) Untreated sample; (b) 2 kW; (c) 4 kW; (d) 6 kW

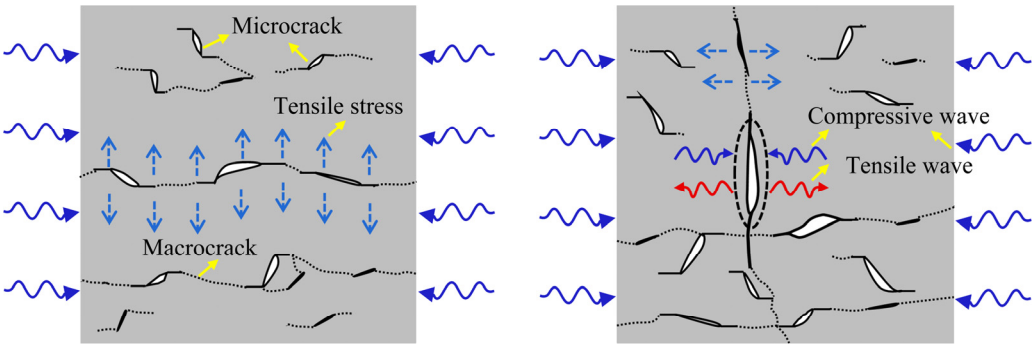

Fig. 12 Typical failure patterns of basalt samples in dynamic compressive tests: (a) Type I: failure with axial splitting cracks; (b) Type II: failure with cracks along axial and perpendicular to axial direction

prolonged exposure time, a large number of microcracks generated and randomly distributed in basalt samples. When the compressive stress wave encounters the opened microcrack, it will be reflected as a tensile wave on the wall surface, which is equivalent to free surface reflection, as shown in Fig. 12. Subsequently, the wave reflection will continuously generate between the incident end and the microcrack, causing a significant increase in tensile stress [38]. The increasing stress intensifies the crack propagation and coalescence, resulting in macrocracks perpendicular to the axial direction. Meanwhile, it is worth noting that the cracks perpendicular to the axial direction occurred later than the axial cracks. This is mainly because the cracks first closed to a certain extent under the impact force, and then expanded under the tensile stress.

5 Discussion

5.1 Pore evolution characteristics of basalt affected by microwave radiation

To investigate the effect of microwave radiation on the microstructure damage of basalt, nuclear magnetic resonance technology (NMR) was utilized in this study. Figure 13 shows the T_2 spectrum of basalt before and after microwave radiation. The abscissa of the T_2 spectrum is the transverse relaxation time, which is proportional to the pore radius. The ordinate of the T_2 spectrum represents the relative content of hydrogen nuclei in water-filled pores, which can reflect the relative volume of pores with corresponding pore size. Therefore, the distribution of the pore radius of the sample can be obtained from the T_2 spectrum. We categorized the pores according to T_2 values into micropores ($T_2 \leq 5$ ms), mesopores (5 ms $\leq T_2 \leq$ 500 ms) and macropores ($T_2 \geq$ 500 ms).

As shown in Fig. 13(a), when the microwave power is 2 kW, the pore distributions of samples treated with different heating time are quite different. Specifically, the majority of pores in the original sample are micropores, followed by mesopores. After being treated for 30 s, the content of micropores in the basalt increased significantly, whereas the content of mesopores did not change much. This indicates that under the microwave radiation within 30 s, the new micropores have begun to form in large numbers due to heterogeneous deformation and loss of water and volatile matters. As the exposure time further increased to 60 and 90 s, there was no significant increase in the content of micropores, but the content of mesopores increased to varying degrees. In this stage, the thermal stress increased enough to promote the expansion of micropores to mesopores. At the same time, new micropores were constantly formed, so the content of micropores in this stage did not change much. When the exposure time reached 120 and 180 s, the content of mesopores continued to increase, and the macropores appeared on a large scale after 180 s. On the contrary, the content of micropores in basalt dropped sharply. This indicated that the micropores in this stage further expanded into larger ones on a larger scale, and the expansion of micropores to mesopores and macropores is the main reason for the decrease in the content of micropores.

As shown in Fig. 13(b), after being treated by microwave at 4 kW, the pore size distributions of the basalt samples changed a lot. Specifically, after

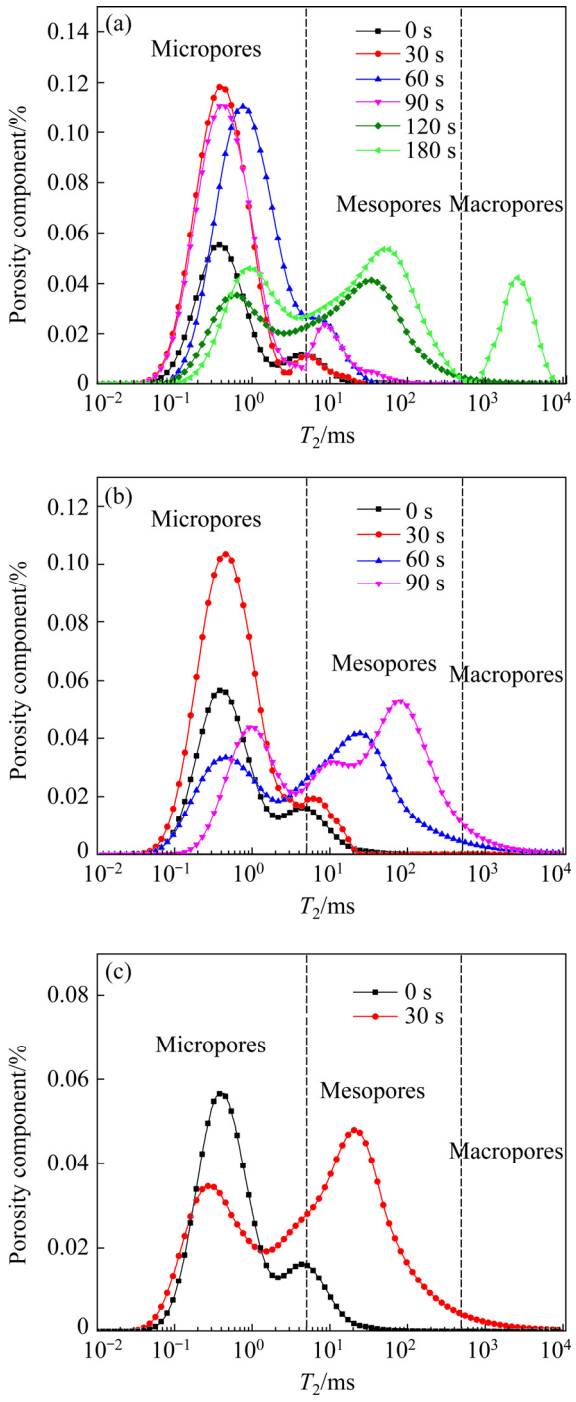

Fig. 13 NMR T_2 spectrum distribution and pore size distribution of basalt before and after microwave radiation: (a) 2 kW; (b) 4 kW; (c) 6 kW

30 s of microwave radiation, the content of micropores increased dramatically, while that of mesopores increased relatively slightly. In this phase, the microwave can sufficiently promote the generation and accumulation of micropores, and can also support the expansion of micropores into mesopores to a certain extent. Compared with the sample treated at 2 kW, the expansion of micropores is more obvious, which indicates that under the same microwave exposure time, the thermal stress caused by expansion mismatch at higher microwave power is larger. As the exposure time increased to 60 and 90 s, the content of mesopores increased sharply, while that of micropores reduced significantly. In this stage, the micropores gradually transformed into mesopores and macropores.

In general, the evolution of pores in the basalt under microwave radiation can be divided into two stages. For a short period of microwave radiation, the evolution of pores is dominated by the generation and accumulation of micropores, while for long-term microwave radiation, the evolution of pores is dominated by the expansion of micropores into mesopores and macropores. During the process of microwave radiation, various kinds of water in the basalt will be constantly dissociated. It is well known that the absorbed water can escape at around 100 °C, the bound water can escape between 150 and 300 °C; and the crystal water can escape at around 400 °C [39,40]. In the first stage, many new micropores appeared and some micropores enlarged into mesopores. Some volatile matters were heated and then escaped from the pore matrix, causing the formation of new pores. Meanwhile, the vapor pressure and thermal stress caused by microwave radiation promoted the initiation of pores and small fractures. In the second stage, pores further developed and began to connect adjacent pores under the combined action of void pressure and thermal stress.

5.2 Damage mechanism of basalt induced by microwave radiation

The damage mechanism of basalt under microwave radiation can be attributed to the difference in mineral dielectric properties and thermal expansion. According to the sensitivity to microwave, the minerals in this basalt can be divided into two categories: strong absorbers (pyroxene) and weak absorbers (feldspar, montmorillonite, quartz). Figure 14 shows a schematic diagram of the damage mechanism of basalt under microwave radiation.

The thermal expansion deformation of the material is positively related to the temperature and the thermal expansion coefficient of the material.

When subjected to microwave radiation, the microwave-heat conversion efficiency of strong absorbers is much higher than that of weak absorbers, which leads to a high heating rate and a higher temperature of the strong absorber. For basalt in this study, the content of pyroxene and feldspar accounts for as much as 92.39%, and the volume thermal expansion coefficients of the former and the latter are 3.4/°C and 2.45/°C, respectively [41,42]. Thus, it is reasonable to think that the thermal expansion coefficient of strong absorbers in basalt is much greater than that of weak absorbers, and this expansion mismatch further leads to thermal stress, known as the thermal shock.

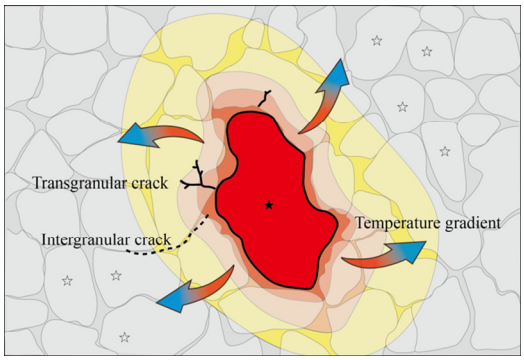

Fig. 14 Schematic diagram of damage mechanism of basalt under microwave radiation (★ represents microwave sensitive mineral; ☆ represents microwave insensitive mineral)

LU et al [8] revealed that microwave-induced microcracks mainly occurred along or through the grains of weak absorbers. Meanwhile, according to the investigation [19,43], when the brittle material is subjected to thermal shock, the compressive stresses are mainly generated in the area with higher temperature, while the tensile stress zone is mainly distributed in the area with lower temperature. Therefore, it can be concluded that microcracks caused by tensile stress are an important cause of microwave-induced thermal damage. The tensile stress (σ_t) of brittle materials caused by thermal shock can be calculated by the following formulas [44]:

$$\sigma_t = \frac{E\alpha\Delta T}{1-\mu} f'_\beta \tag{9}$$

$$f'_\beta = \frac{1}{a/\beta + b - c\mathrm{e}^{-d/\beta}} \tag{10}$$

$$\beta = \frac{Rh}{\lambda} \tag{11}$$

where α and λ are the thermal expansion coefficient and thermal conductivity, respectively, h is the contact heat transfer coefficient; R is the characteristic heat transfer length; E and μ are the elastic modulus and Poisson's ratio; a, b, c, and d are constants.

From Eqs. (9)−(11), f'_β is a monotonically increasing function, and σ_t has a positive correlation with h and ΔT [44]. The tensile stress caused by thermal shock is mainly determined by mineral properties, temperature difference and contact thermal conductivity. After microwave radiation, the temperature of strong absorbing minerals is significantly higher than that of weak absorbing minerals, and the higher the microwave power and the longer the heating time, the greater the temperature difference between strong absorbers and weak absorbers. Meanwhile, the increased temperature difference promotes the heat transfer rate and thus increases the heat transfer coefficient [45,46]. Under the combined effects of the mentioned two factors, the higher the microwave power and the longer the heating time, the greater the tensile stress caused by thermal shock. In addition, the cohesion between the mineral particles is generally much smaller than that within the mineral particles. Therefore, when the thermal stress exceeds the ultimate strength, the transgranular and intergranular cracks generate successively.

5.3 Microwave applications in drilling

Today, advanced drilling methods based on thermal and ablative effects utilize technologies such as microwaves, lasers, plasma jets, flames, and electric heaters [47]. In particular, the microwave has been widely used for the processing of various materials due to its high efficiency and environmental friendliness.

The main technical principle of microwave drilling is to concentrate microwave energy on a small spot, called hot spot, where microwave energy is dissipated into the rock in form of heat to pre-degrade the rock. As illustrated in Fig. 15(a), microwaves are generated by magnetrons and then transmit to the hot spot through the waveguide and antenna. After the material is softened, the drill bit can be inserted into the work piece, and the diameter

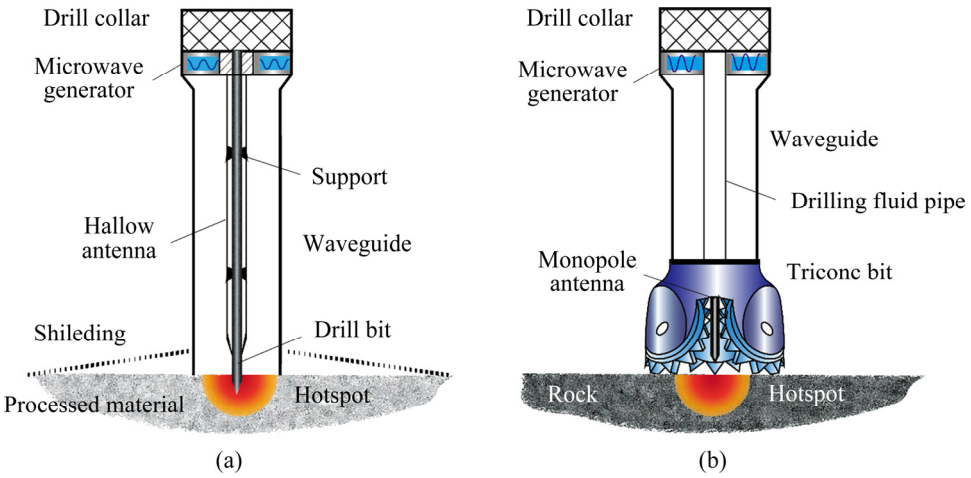

Fig. 15 Schematic diagram of microwave drilling equipment: (a) Equipment for fine processing of small diameter and shallow holes [48]; (b) Equipment for mining and geological drilling of larger diameter and medium-deep drill hole

of the hole is limited by the size of the antenna. In 2002, JERBY [48] first proposed a drilling method that uses near-field microwave radiation to generate localized hot spots, which can drill holes with a diameter of 0.5 mm. For large-diameter and deep holes mostly used in the mining and construction industries, the antenna can be placed inside the drill bit to achieve simultaneous operation of microwave degradation and mechanical drilling. As shown in Fig. 15(b), the device consists of three main modules: a microwave heating unit to pre-weaken the rock mass, a mechanical drilling rig unit to achieve subsequent drilling, and a water jet unit to remove cuttings and reduce operating temperature. This device realizes a combination of mechanical, thermal, and hydraulic power for rock breaking.

LESTER and KINGMAN [49] exposed lead−zinc to microwave with a power of 15 kW for only 1 s. As a result, less than 55% of the original strength remained. HARTLIEB and GRAFE [50] found that the cutting force of granite dropped by 10% after 30 s in a 24 kW open-ended waveguide. Actually, reasonable determination of microwave power, frequency and exposure time is the key to improving microwave efficiency. Moreover, the economic performance of microwave-assisted rock breaking has always been concerned by scholars. KINGMAN et al [12,51,52] conducted electric crushing experiments on ores before and after microwave radiation to achieve the same degree of crushing, founding that crushing the ores pretreated by microwave can reduce energy consumption by about 50%.

For further industrial applications of the microwaves, it is necessary to meet the technical requirements of microwave-assisted mechanical equipment, including the design of microwave-assisted drilling device, the control of electro-magnetic radiation risks and the miniaturization of equipment.

6 Conclusions

(1) The heating rates on the surface of basalt samples under microwave at 2, 4 and 6 kW are 1.65, 1.98 and 3.58 °C/s, respectively. The ultrasonic detection tests show that both increased power levels and prolonged exposure time can cause severer damage to the basalt.

(2) As the microwave power level and exposure time increase, the dynamic compressive strength of the treated basalt continues to decrease, while the peak strain continues to increase. The failure mode of the treated basalt under impact stress gradually changes from an axial splitting to a compound failure mode, which is attributed to the combined effects of reflected tension waves and the Poisson effect.

(3) With increasing microwave exposure time, the P-wave velocity of microwave-treated basalt decreases continuously. For a short period of microwave radiation, the formation and accumulation of micropores dominate, while for a long period of microwave radiation, the expansion of micropores into mesopores and macropores dominate.

(4) The tensile stress caused by thermal shock is an important reason for the generation and expansion of microcracks in basalt under microwave radiation. Increasing the microwave power level and exposure time to enlarge the temperature difference between microwave sensitive minerals and insensitive minerals can effectively increase the amount of damage in basalt, which can induce a severer degradation of basalt.

Acknowledgments

This work was supported by the National Natural Science Foundation of China (Nos. 51774325, 41972283, 11972378).

References

[1] LI Xi-bing, YAO Jin-rui, DU Kun. Preliminary study for induced fracture and non-explosive continuous mining in high-geostress hard rock mine—A case study of kaiyang phosphate mine [J]. Chinese Journal of Rock Mechanics and Engineering, 2013, 32(6): 1101−1111. (in Chinese)

[2] WANG Shao-feng, TANG Yu, LI Xi-bing, DU Kun. Analyses and predictions of rock cuttabilities under different confining stresses and rock properties based on rock indentation tests by conical pick [J]. Transactions of Nonferrous Metals Society of China, 2021, 31(6): 1766−1783.

[3] WANG Pin, YIN Tu-bing, HU Bi-wei, Dynamic tensile strength and failure mechanisms of thermally treated sandstone under dry and water-saturated conditions [J]. Transactions of Nonferrous Metals Society of China, 2020, 30(8): 2217−2238.

[4] WANG Shao-feng, SUN Li-cheng, HUANG Lin-qi, LI Xi-bing, SHI Ying, YAO Jin-rui, DU Shao-lun. Non-explosive mining and waste utilization for achieving green mining in underground hard rock mine in China [J]. Transactions of Nonferrous Metals Society of China, 2019, 29(9): 1914−1928.

[5] LU Gao-ming, FENG Xia-ting, LI Yuan-hui, ZHANG Xi-wei. The microwave-induced fracturing of hard rock [J]. Rock Mechanics and Rock Engineering, 2019, 52(9): 3017−3032.

[6] JONES D A, KINGMAN S W, WHITTLES D N, LOWNDES I S. Understanding microwave assisted breakage [J]. Minerals Engineering, 2005, 18(7): 659−669.

[7] JONES D A, KINGMAN S W, WHITTLES D N, LOWNDES I S. The influence of microwave energy delivery method on strength reduction in ore samples [J]. Chemical Engineering and Processing: Process Intensification, 2007, 46(4): 291−299.

[8] LU Gao-ming, LI Yuan-hui, HASSANI F, ZHANG xi-wei. The influence of microwave irradiation on thermal properties of main rock-forming minerals [J]. Applied Thermal Engineering, 2017, 112: 1523−1532.

[9] CHEN T T, DUTRIZAC J E, HAQUE K E, WYSLOUZIL W, KASHYAP S. The relative transparency of minerals to microwave radiation [J]. Canadian Metallurgical Quarterly, 1984, 23(3): 349−351.

[10] ALI A Y, BRADSHAW S M. Quantifying damage around grain boundaries in microwave treated ores [J]. Chemical Engineering and Processing: Process Intensification, 2009, 48(11/12): 1566−1573.

[11] HASSANI F, NEKOOVAGHT P M, GHARIB N. The influence of microwave irradiation on rocks for microwave-assisted underground excavation [J]. Journal of Rock Mechanics and Geotechnical Engineering, 2016, 8(1): 1−15.

[12] KINGMAN S W, JACKSON K, BRADSHAW S M, ROWSON N A, GREENWOOD R. An investigation into the influence of microwave treatment on mineral ore comminution [J]. Powder Technology, 2004, 146(3): 176−184.

[13] LI Qiang, LI Xi-bing, YIN Tu-bing. Effect of microwave heating on fracture behavior of granite: An experimental investigation [J]. Engineering Fracture Mechanics, 2021, 250: 107758.

[14] PEINSITT T, KUCHAR F, HARTLIEB P, MOSER P, KARGL H, RESTNER U. Microwave heating of dry and water saturated basalt, granite and sandstone [J]. International Journal of Mining and Mineral Engineering, 2010, 2: 18−29.

[15] WANG Yi-cai, DJORDJEVIC N. Thermal stress FEM analysis of rock with microwave energy [J]. International Journal of Mineral Processing, 2014, 130: 74−81.

[16] ALI A Y, BRADSHAW S M. Bonded-particle modelling of microwave-induced damage in ore particles [J]. Minerals Engineering, 2010, 23(10): 780−790.

[17] OMRAN M, FABRITIUS T, ELMAHDY A M, ABDEL-KHALEK N A, EL-AREF M, ELMANAWI A E H. XPS and FTIR spectroscopic study on microwave treated high phosphorus iron ore [J]. Applied Surface Science, 2015, 345: 127−140.

[18] HARTLIEB P, GRAFE B, SHEPEL T, MALOVYK A, AKBARI B. Experimental study on artificially induced crack patterns and their consequences on mechanical excavation processes [J]. International Journal of Rock Mechanics and Mining Sciences, 2017, 100: 160−169.

[19] KINGMAN S W, CORFIELD G M, ROWSON N A. Effects of microwave radiation upon the mineralogy and magnetic processing of a massive norwegian ilmenite ore [J]. Magnetic and Electrical Separation, 1999, 3(9): 131−148.

[20] TOIFL M, MEISELS R, HARTLIEB P, KUCHAR F, ANTRETTER T. 3D numerical study on microwave induced stresses in inhomogeneous hard rocks [J]. Minerals Engineering, 2016, 90: 29−42.

[21] JOHN R S, BATCHELOR A R, IVANOV D, UDOUDO O B, JONES D A, DODDS C, KINGMAN S W. Understanding microwave induced sorting of porphyry copper ores [J]. Minerals Engineering, 2015, 84: 77−87.

[22] LI Xi-bing, ZHOU Zi-long, LOK T S, HONG Liang, YIN Tu-bing. Innovative testing technique of rock subjected to coupled static and dynamic loads [J]. International Journal of Rock Mechanics and Mining Sciences, 2008, 45(5): 739−748.

[23] HASSANPOUR J, ROSTAMI J, ZHAO Jian, AZALI S T. TBM performance and disc cutter wear prediction based on ten years experience of TBM tunnelling in Iran [J]. Geomechanics and Tunnelling, 2015, 8(3): 239−247.

[24] LI Xi-bing, WANG Shao-feng, WANG Shan-yong. Experimental investigation of the influence of confining stress on hard rock fragmentation using a conical pick[J]. Rock Mechanics and Rock Engineering, 2018, 5(1): 255−277.

[25] ERGIN H, ACAROGLU O. The effect of machine design parameters on the stability of a roadheader [J]. Tunnelling and Underground Space Technology, 2007, 22(1): 80−89.

[26] YANG Dao-long, LI Jian-ping, WANG Li-ping, GAO Kui-dong, TANG You-hong, WANG Yan-xiang. Experimental and theoretical design for decreasing wear in conical picks in rotation-drilling cutting process [J]. The International Journal of Advanced Manufacturing Technology, 2015, 77(9/10/11/12): 1571−1579.

[27] ZHOU Ying-xin, XIA Kai-wen, LI Xi-bing, LI Hai-bo, MA Guo-wei, ZHAO Jian, ZHOU Zi-long, DAI Feng. Suggested methods for determining the dynamic strength parameters and mode-I fracture toughness of rock materials [J]. International Journal of Rock Mechanics and Mining Sciences, 2012, 49: 105−112.

[28] ZHOU Zi-long, CAI Xin, CHEN Lu, CAO Wen-zhuo, ZHAO Yuan, XIONG Cheng. Influence of cyclic wetting and drying on physical and dynamic compressive properties of sandstone [J]. Engineering Geology, 2017, 220: 1−12.

[29] LI Jie-lin, HONG Liu, ZHOU Ke-ping, XIA Cai-chu, ZHU Long-yin. Mechanical characteristics and mesostructural damage of saturated limestone under different load and unload paths [J]. Advances in Civil Engineering, 2021, 2021: 1−16.

[30] LI Xi-bing, LIU De-shun, GU De-sheng. Effective method of eliminating the oscillation of rock dynamic stress-strain curves [J]. Journal of Central South University of Technology, 1995(4): 457−460. (in Chinese)

[31] DAI Feng, HUANG Sheng, XIA Kai-wen, TAN Zhuo-ying. Some fundamental issues in dynamic compression and tension tests of rocks using split Hopkinson pressure bar[J]. Rock Mechanics and Rock Engineering, 2010, 43(6): 657−666.

[32] ZHANG Q B, ZHAO J. A review of dynamic experimental techniques and mechanical behaviour of rock materials[J]. Rock Mechanics and Rock Engineering, 2014, 47(4): 1411−1478.

[33] ZHENG Yan-long, ZHANG Qian-bing, ZHAO Jian. Effect of microwave treatment on thermal and ultrasonic properties of gabbro [J]. Applied Thermal Engineering, 2017, 127: 359−369. DOI: http://dx.doi.org/10.1016/j.applthermaleng.2017.08.060.

[34] ZHENG Yan-long, MA Zhong-jun, ZHAO Xiao-bao, HE Lei. Experimental investigation on the thermal, mechanical and cracking behaviours of three igneous rocks under microwave treatment [J]. Rock Mechanics and Rock Engineering, 2020, 53(8): 3657−3671.

[35] LIU Shi, XU Jin-yu. An experimental study on the physico-mechanical properties of two post-high-temperature rocks [J]. Engineering Geology, 2015, 185: 63−70.

[36] ZHOU Zi-long, CAI Xin, LI Xi-bing, CAO Wen-zhuo, DU Xue-ming. Dynamic response and energy evolution of sandstone under coupled static−dynamic compression: Insights from experimental study into deep rock engineering applications [J]. Rock Mechanics and Rock Engineering, 2020, 53(3): 1305−1331.

[37] HU Bi-wei, YIN Tu-bing, LI Xi-bing. Experimental study on mechanical impact breaking rock with microwave radiation [J]. Gold Science and Technology, 2020, 28(4): 521−530. (in Chinese)

[38] CADONI E, LABIBES K, ALBERTINI C, BERRA M, GIANGRASSO M. Strain-rate effect on the tensile behaviour of concrete at different relative humidity levels [J]. Materials and Structures, 2001, 34: 21−26.

[39] ZHANG Wei-qiang, SUN Qiang, HAO Shu-qing, GENG Ji-shi, LV Chao. Experimental study on the variation of physical and mechanical properties of rock after high temperature treatment [J]. Applied Thermal Engineering, 2016, 98: 1297−1304.

[40] SUN Qiang, LÜ Chao, CAO Li-wen, LI Wei-chao, GENG Ji-shi, ZHANG Wei-qiang. Thermal properties of sandstone after treatment at high temperature [J]. International Journal of Rock Mechanics and Mining Sciences, 2016, 85: 60−66.

[41] TRIBAUDINO M, NESTOLA F, BRUNO M, BALLARAN T B, LIEBSKE C. Thermal expansion along the $NaAlSi_2O_6$−$NaFe_3+Si_2O_6$ and $NaAlSi_2O_6$−$CaFe_2+Si_2O_6$ solid solutions [J]. Physics and Chemistry of Minerals, 2008, 35(5): 241−248.

[42] TRIBAUDINO M, BRUNO M, NESTOLA F, PASQUAL D, ANGEL R J. Thermoelastic and thermodynamic properties of plagioclase feldspars from thermal expansion measurements [J]. American Mineralogist, 2011, 96(7): 992−1002.

[43] KIM K, KEMENY J, NICKERSON M. Effect of rapid thermal cooling on mechanical rock properties [J]. Rock Mechanics and Rock Engineering, 2014, 47(6): 2005−2019.

[44] COLLIN M, ROWCLIFFE D. Analysis and prediction of thermal shock in brittle materials [J]. Acta Materialia, 2000, 48(8): 1655−1665.

[45] GIBSON R D. The contact resistance for a semi-infinite cylinder in a vacuum [J]. Applied Energy, 1976, 2(1): 57−65.

[46] MIKIC B, CARNASCIALI G. The effect of thermal conductivity of plating material on thermal contact resistance [J]. Journal of Heat Transfer, 1970, 92(3): 475−481.

[47] JERBY E, DIKHTYAR V, AKTUSHEV O. The microwave-drill technology [C]//23rd IEEE Convention of Electrical and Electronics Engineers in Israel. Tel-Aviv, Israel: IEEE, 2004: 269−272. DOI: https://doi.org/10.1109/EEEI.2004. 1361143.

[48] JERBY E. The microwave drill [J]. Science, 2002, 5593(298): 587−589.

[49] LESTER E, KINGMAN S. The effect of microwave pre-heating on five different coals [J]. Fuel, 2004, 83(14/15): 1941−1947.

[50] HARTLIEB P, GRAFE B. Experimental study on microwave assisted hard rock cutting of granite[J]. BHM Berg-Und Hüttenmännische Monatshefte, 2017, 162(2): 77−81.

[51] KINGMAN S W, JACKSON K, CUMBANE A, BRADSHAW S M, ROWSON N A, GREENWOOD R. Recent developments in microwave-assisted comminution [J]. International Journal of Mineral Processing, 2004, 74(1/2/3/4): 71−83.
[52] KINGMAN S W, VORSTER W, ROWSON N A. The influence of mineralogy on microwave assisted grinding [J]. Minerals Engineering, 2000, 13(3): 313−327.

微波辐射对玄武岩动态压缩性能的影响

尹土兵，金飞燕，李 檣，李夕兵

中南大学 资源与安全工程学院，长沙 410083

摘 要：通过 SHPB 系统研究微波对玄武岩动态力学性能的影响，同时借助超声无损检测和核磁共振技术表征玄武岩热损伤情况。结果表明，随着微波功率和辐射时间的增加，P 波波速、动态抗压强度和弹性模量不断降低，动态破坏模式趋于复杂。增大微波功率和辐射时间可提高矿物间的温差和传热系数，进而加剧热冲击对岩石造成的损伤。

关键词：微波辐射；核磁共振；动态压缩性能；热损伤

(Edited by Xiang-qun LI)